Version of Record: https://www.sciencedirect.com/science/article/pii/S0927775722020568
Manuscript_a36fb7b468d724370e288cc3c9d6f5d6

# Molecular simulation of the structural and thermodynamic properties of n-alkane/brine interfacial systems with nonionic surfactants

Gabriel D. Barbosa[1], Arthur M. Luz[2], Carla L. M. Camargo[2], Frederico W. Tavares[2,3], C. Heath Turner[1†]

[1] Department of Chemical and Biological Engineering, The University of Alabama, Tuscaloosa, AL 35487

[2] Escola de Química, Universidade Federal do Rio de Janeiro, Rio de Janeiro, RJ, Brasil

[3] Programa de Engenharia Química - PEQ/COPPE, Universidade Federal do Rio de Janeiro, Rio de Janeiro, RJ, Brasil

**†Corresponding Author:**
E-mail: hturner@eng.ua.edu
Phone: +1 (205) 348-1733

**Abstract**

All-atom molecular dynamics (MD) simulations are used to study the structural and thermodynamic properties of water + n-heptane interfacial systems in the presence of salinity (NaCl, NaI, KCl, and KI) and two different nonionic surfactants. Excellent qualitative and quantitative agreement with interfacial tension experimental data is obtained, but this requires applying a charge scaling factor to the ionic species, suggesting the likely role of polarizability effects. Tensoactive behavior is observed for the NaI and KI systems, coinciding with layering of the iodide species near the interface. There are significant interaction differences between the surfactants and the different ionic species, but the structural and thermodynamic behavior of the surfactant molecules is relatively unaffected by the specific salt species. Our analysis suggest that the surfactant-surfactant interactions play a critical role in determining the interfacial behavior, with a much smaller impact associated with the composition of the brine phase.

**Keywords**: interface; surfactants; free-energy; phase behavior; molecular dynamics

## 1. Introduction

Inhomogeneous systems are of great importance in several industrial fields. For instance, with regards to water flooding processes for enhanced oil recovery (EOR), there is a clear need for systematic studies that identify ways to control interfacial tension and wettability. Due to their amphiphilic nature, surfactants injected during water flooding improve oil removal from reservoirs; several mechanisms have been proposed to explain the role of the surfactants.[1–3] Besides surfactants, the presence of ionic species also influences the interactions between the oil and water phases. The change in rock wettability caused by the salinity of the aqueous phase is an important mechanism involved in EOR. However, salinity also affects the fluid-fluid interactions and oil-water interfacial tension in complex ways, since there are a variety of compounds present in the oil phase, specifically those containing acid sites.[4,5]

Due to their low toxicity, sorbitan oleates (Spans) and polyoxyethylene sorbitan fatty acid esters (Tweens) are commercial surfactants widely used in the pharmaceutical, cosmetic, and food industries.[6–10] Their emulsification capacity and effect on rheology and kinetics of interfacial properties have been experimentally studied in detail.[11–14] For instance, Capdevila et al.[15] identified the influence of surfactant:oil ratio and length of the carbon tail on the stability of highly concentrated water/oil/Span 80 emulsions. Bak et al.[16] reported measurements of the interfacial tension of toluene/water and air/water systems in the presence of different types of Tweens. Cao et al.[17] evaluated the effect of these surfactants' molecular structure on emulsions' stability, verifying higher stability with increased tail length and decreased number of

unsaturated bonds. The synergistic effects of these surfactants on emulsion stability have also been investigated, due to their different affinities for water and oil phases.[18]

The aggregation behavior of surfactants is generally affected by the presence of salts. Although electrostatic interactions do not contribute to the micellization free energy of non-ionic surfactants, the presence of salts can affect the solubility of the tail and head of the surfactant. Therefore, the activity coefficients estimated from these solubility values are also modified by the presence of salts. Besides, even though the heads of nonionic surfactant are charge-neutral, it has been shown that the adsorption of ionic species within the interfacial region can play an important role in the overall interfacial behavior.[19] In a combined theoretical-experimental study of polyethoxylated alcohol-type surfactants ($C_xEO_y$), Carale et al.[20] concluded that salts have a more pronounced effect on the hydrophobic chain in relation to the hydrophilic head, causing a decrease in the solubility of alkyl groups. Experiments also showed a decrease in CMC and surface tension in the presence of salts. Also, Al-Sabagh et al.[21] found that the presence of salts tends to decrease the cloud point temperature, and this was also observed in the experiments reported by Hadji et al.[22] for alkyl ether/brine systems.

According to Imperatore et al.,[23] the presence of inorganic electrolytes affects the aggregation behavior of surfactants, modifying intramolecular and intermolecular interactions. For ionic surfactants, the aggregation mechanisms can be explained in terms of electrostatic interactions, while for non-ionic surfactants these mechanisms are still not well understood. The authors used pulsed gradient spin-echo NMR to determine the self-diffusion coefficients in a mixture of several alkaline and alkaline-earth metal chlorides. The results showed that for

$C_xEO_y$ surfactants, the presence of electrolytes caused a decrease in the CMC, although the micelle size was unaffected. These results were attributed to the dehydration of the alkyl chains and the ethoxylated chains.

Molecular dynamics (MD) simulations are a powerful tool for investigating several interfacial phenomena, namely, the packing of surfactants within the interfacial monolayer,[24] the effect of nanoparticles and surfactants on interfacial tension (via coarse-grained simulations),[25,26] and even the electrocoalescence of water droplets in the presence of surfactants.[27] In addition, MD can be used to directly investigate ionic specificity effects.[28–30] More specifically, Underwood et al.[31] evaluated different force fields to calculate the interfacial properties of a water/decane/NaCl system. In other work, Abdel-Azeim et al.[32] investigated the effect of organic acids and divalent ions at the brine/oil interface. By combining both surfactants and ions, several authors have obtained a more realistic picture of water/oil interfacial systems, specifically with regards to interfacial tension characterization and the study of the impact of ionic strength on the interfacial structure. Nan et al.[33] assessed the effects of charge and concentration of ions at the sodium dodecyl sulfate (SDS) monolayer. Riccardi et al.[34] focused on the AOT (dioctyl sodium sulfosuccinate) ionic surfactant, concluding that divalent ions (e.g., calcium) cause inhomogeneities in the interfacial occupation due to clustering behavior from electrostatic interactions. Finally, Alonso et al.[35] investigated the effect of inorganic ions coupled with polyoxyethylene nonionic surfactants on the interfacial tension of water/oil systems, observing that cations primarily interact with the head groups altering the organization of surfactants at the interface. These changes in the interfacial region disrupt water/dodecane and water/surfactant interactions, altering the interfacial tension of the overall system.

Although several studies have attempted to correlate the macroscopic properties of interfacial systems to their behavior at a molecular level using MD simulations, little effort has been made to investigate the synergistic effects between surfactants and ions, specifically for nonionic surfactants. In this work, we use all-atom MD simulations to study water + n-heptane interfacial systems in the presence of both salinity and two different nonionic surfactants. Despite structural differences, some Span and Tween-type surfactants maintain similar features. For example, Span 80 and Tween 80 contain the same unsaturated hydrophobic tail, but only Tween 20 has an ethoxylated head. Similarly, Span 20 and Tween 20 have the same saturated hydrophobic tail, but the Tween 20 head contains ethylene oxides. In this work, we chose Span 80 and 2-(2-(3,4-bis(2-hydroxyethoxy)tetrahydrofuran-2-yl)-2-(2-hydroxyethoxy)ethoxy)ethyl dodecanoate (TED) to investigate how salinity affects these commercial surfactants. We used a TED surfactant to avoid a large difference in hydrophilicity with respect to the Span 80 surfactant. The ion specificity for different ionic pairs is evaluated at three different surfactant concentrations, as well as analyses of interfacial tension, interfacial structure (i.e., density distributions), surfactant tilt angles, and hydrogen bonding. Furthermore, we quantify the transfer free energy of the surfactant molecules across bulk phases (passing through the interfacial region), by calculating the potential of mean force (PMF). Based on the PMFs, we evaluate the solubility free energy differences, and therefore, the affinity of the surfactants within each phase.

## 2. Molecular Simulation Methodology

Here, Gromacs 2021.1 is used to perform the MD simulations.[36,37] The non-bonded and bonded interactions of the studied surfactants and n-heptane are modeled using the OPLS-AA

force field;[38–40] the SPC/E water model is used to model water interactions.[31,41] The force field parameters are obtained using the LigParGen web-server,[38] and consistent with the OPLS-AA force field, geometric mixing rules are used to obtain unlike pair interactions. Before initiating the classical MD simulations, the molecular structures are optimized using density functional theory at the B3LYP/6-31+(d,p) level of theory using Gaussian09.[42] Figure S1 shows the electrostatic surface map of Span 80 and TED. Then, based on the optimized structures, the 1.2*CM5 method is used to calculate the partial atomic charges.[43,44] Notably, it was shown before that the combination of the 1.2*CM5 method and the OPLS-AA force field leads to good predictions of the thermodynamic properties of several organic compounds.[43] Consistent with the OPLS-AA force field, a cut-off radius of 1.0 nm is used for the Lennard-Jones (LJ) and coulombic interactions. Due to the inhomogeneity of the interfacial systems, the Particle Mesh Ewald (PME)[45] method is used to calculate the long-range corrections to both the LJ and coulombic interactions. In the simulations performed here, H-bonds are constrained using the LINCS algorithm. A time step of 2 fs is used; periodic boundary conditions are applied in all directions, and the leapfrog algorithm is used to integrate the equation of motion. The key features of the Gromacs input and topology files are included as Supporting Information.

To investigate the influence of the ionic species' force field on the description of the interfacial properties, we evaluate the default force field distributed in Gromacs 2021.1 (i.e., the standard OPLS-AA force field),[36,46–48] as well as the force field proposed by Joung and Cheatham.[49] We also quantify the impact of charge scaling on the OPLS-AA force field. Over the past few years, charge scaling has proved to be a computationally efficient strategy for approximating polarizability effects when using fixed-charge force fields.[50–52] Notably, scaling

factors ranging from 0.70 to 0.90 for monovalent ionic species have been proposed to improve monovalent halides' simulation accuracy. A scaling factor of 0.85 is applied to the ionic species in the current work (i.e., the anions and cations possess net charges of -0.85 e and +0.85 e, respectively), which is consistent with the charge scaling factor recently used by Zeron et al.[50] Here, for brevity, these three force fields (original OPLS-AA force field, force field proposed by Joung and Cheatham, and OPLS-AA force field with the scaling factor) are labeled OPLS-AA, JC, and sOPLS-AA.

The Packmol package[53] is used to obtain the initial configurations of the interfacial systems; the aqueous and oil phases are constructed with 10,000 and 1,000 molecules of water and n-heptane, respectively. To understand the interfacial behavior of the Span 80 and TED surfactants interacting with different aqueous phase compositions, we consider four different brine compositions (NaCl, NaI, KCl, and KI), in which the bulk concentrations of the ionic species were chosen based on the experimental study of Lima et al.;[54] besides, three different surfactant superficial concentrations were used: 0, 24, and 48 surfactant molecules. Table 1 provides a summary of the simulated system compositions.

**Table 1.** Number of molecules of each compound in the simulated systems.

| System | Water | n-Heptane | Salt | Surf. |
|---|---|---|---|---|
| nHept/W | 10,000 | 1,000 | - | 0/24/48 |
| nHept/NaCl | 10,000 | 1,000 | 282 | 0/24/48 |
| nHept/NaI | 10,000 | 1,000 | 288 | 0/24/48 |
| nHept/KCl | 10,000 | 1,000 | 287 | 0/24/48 |

| | | | | |
|---|---|---|---|---|
| nHept/KI | 10,000 | 1,000 | 294 | 0/24/48 |

Based on the initial configurations, the steepest descent method is used to minimize the energy of the system, followed by an isothermal–isobaric ensemble (NPT) equilibration stage of 50 ns. The Parrinello-Rahman barostat[55,56] and v-rescale thermostat[57] are used to maintain the constant pressure and temperature conditions, with time constants of 5 ps and 0.1 ps, respectively. Simulation runs of 100 ns in the canonical (NVT) ensemble are used for sampling purposes.

To evaluate surfactant ordering in the interfacial region, the structure factor along the z-direction is calculated using the MDAnalysis package according to

$$S_z(z) = \frac{1}{2}(3\langle cos^2(\theta)\rangle - 1)\,, \qquad (1)$$

in which $\theta$ is the angle between a vector connecting two adjacent atoms and the z-axis unit vector ($\hat{\mathbf{e}}_z$). According to Eq. 1, $S_z$ approaches 1.0 when the chosen vector is parallel to the z-axis, and it is -0.5 when the vector is perpendicular.[58] Figure 1 shows the chosen vector assignments within the Span 80 and TED structures. Here, the geometric center of the initial and final sites connecting the vectors in Figure 1 is used as a reference point to define the order parameter profiles. The interfacial tension ($\gamma$) is calculated using the approach of Kirkwood-Irving

$$\gamma = \frac{1}{2}L_z(P_{zz} - \frac{1}{2}(P_{xx} + P_{yy}\ ))\,. \qquad (2)$$

In this equation, $P_{ii}$ is the $ii$ component of the pressure tensor (calculated using the *gmx energy* package within Gromacs), and $L_z$ is the box length in the z-dimension. Similarly, the average

density profiles and H-bond analyses are carried out using *gmx density* and *gmx hbonds,* respectively. The H-bond lifetime is quantified by first calculating the autocorrelation function

$$C(t) = \langle s_{ij}(t_0) s_{ij}(t+\tau) \rangle / \langle s_{ij}(t_0)^2 \rangle \,, \tag{3}$$

in which $s_{ij}$ is 1 if there is a hydrogen bond present and 0 otherwise. The H-bond lifetime ($\tau_{HB}$) is obtained by integrating $C(t)$. To do this, $C(t)$ is first fit to a multiple exponential function

$$C(t) = \sum_i a_i exp(-b_i\, t) \,, \tag{4}$$

in which $a_i$ and $b_i$ are fitting parameters. Then, $\tau_{HB}$ is explicitly calculated as

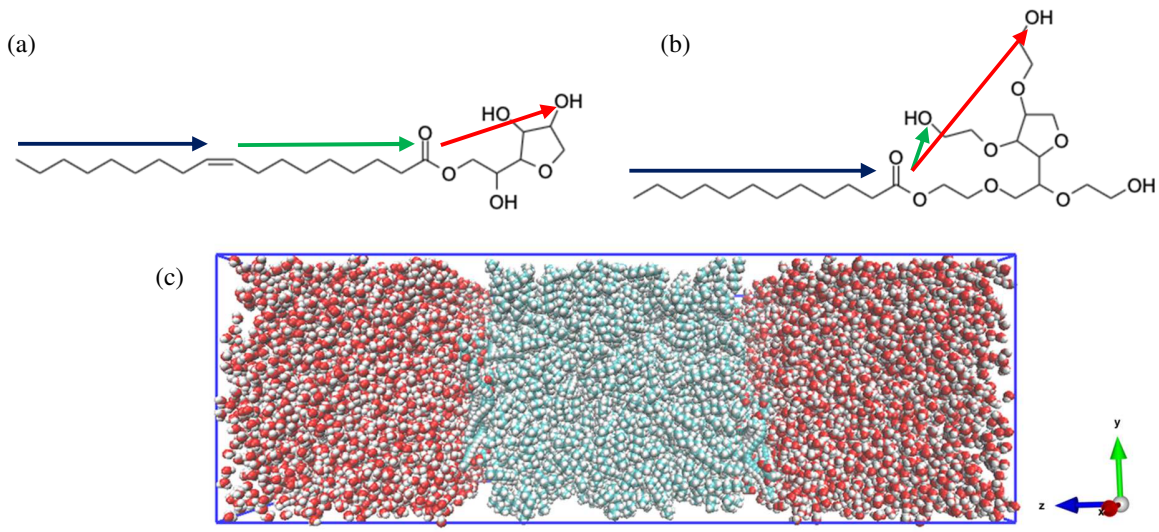


$$\tau_{HB} = \int_0^\infty dt C(t) \,. \tag{5}$$

**Figure 1.** Molecular structure of (a) Span 80 and (b) TED surfactants, and the vectors used to evaluate the structure factor in Eq. (1). Vector color codes: blue = $\mathbf{v_1}$, green = $\mathbf{v_2}$, and red = $\mathbf{v_3}$. (c) Initial configuration of nHept/W with 24 Span 80 molecules (7×7×18 nm$^3$); color code: cyan = carbon; white = hydrogen; red = oxygen.

The partition coefficients of Span 80 and TED are analyzed at infinite dilution conditions in the different interfacial systems by calculating the PMF. In the PMF calculations, the aqueous and oil phases are composed of the same number of water, salt, and n-heptane molecules as shown in Table 1. The umbrella sampling method[59] is used to obtain the PMF, and the weighted histogram analysis method (WHAM)[60], as implemented in *gmx wham,* is used to estimate the PMF based on the biased simulations. In the PMF simulations, we define the reaction coordinate as the z-component of the distance between the center-of-mass of the n-heptane phase and the surfactant molecule.[61] Following this approach, a satisfactory probability distribution overlap is obtained by using a spacing of 0.1 nm between each simulation window, along with a spring constant of 1000 kJ/mol $m^2$. The umbrella sampling simulations are performed using the same parameters and models described above; reasonable PMF estimates are obtained using 5 ns of equilibration followed by 15 ns of production. Finally, bootstrap analysis is used to calculate the statistical confidence region of the obtained PMFs.[62]

## 3. Simulation Results

### *3.1 Interfacial properties of n-heptane/brine systems*

Table 2 shows the effect of the aqueous phase composition and the force field of the ionic species on the interfacial tension for the system with no surfactants. The results obtained for the nHept/W system show remarkable agreement with experimental data published previously (50.7 mN/m).[54,63,64] Concerning the n-heptane/brine systems, both OPLS-AA and JC force fields predict a positive difference between the interfacial tension of the nHept/W and nHept/brine systems ($\Delta\gamma^i = \gamma_{nHept/i} - \gamma_{nHept/W}$), along with an overall trend of $\Delta\gamma^{NaCl} > \Delta\gamma^{NaI} >$

$\Delta\gamma^{KCl} > \Delta\gamma^{KI}$ for the JC force field. Although $\Delta\gamma$ is slightly overestimated for the nHept/NaCl system, both JC and OPLS-AA show good agreement with the experimental data reported by Lima et al.[54] However, the experimentally-obtained[54] tensoactive behavior ($\Delta\gamma < 0$) of the NaI and KI systems is not adequately captured by these two ionic force fields (JC and OPLS-AA). On the other hand, the results obtained using the charge scaling approach (sOPLS-AA) lead to a significant reduction of the predicted $\Delta\gamma$. This leads to a smaller deviation for $\Delta\gamma^{NaCl}$, and a negative $\Delta\gamma$ is obtained for the nHept/NaI and nHept/KI systems, resembling the experimental data. These results support the practice of charge-scaling as a means for approximating polarization effects, and this may be important for future studies when modeling similar interfacial systems.

Figure S2 presents the density distributions along the z-dimension of the simulation boxes for nHept/NaCl, nHept/NaI, nHept/KCl, and nHept/KI, based on the sOPLS-AA force field. In all systems, well-developed bulk aqueous and oil phases are observed, with distinct n-heptane/brine interfacial regions; ion aggregation in the aqueous phase is not observed in any of the evaluated systems. For the nHept/NaCl and nHept/KCl systems, which exhibit $\Delta\gamma > 0$, no significant ion layering is present in the interfacial region. Conversely, much more pronounced ion structuring is observed for the KI and NaI systems. This is explicitly observed by looking at Figure S2 (e), which shows the density profiles of NaCl, NaI, KCl, and KI for the systems with no surfactant in the same plot. Figure S3 shows the prediction for the nHept/KI system based on the OPLS-AA force field: no appreciable layering of KI is observed when no scaling is used, similar to the results of the nHept/NaCl and nHept/KCl systems presented in Figure S2. The comparison of OPLS-AA and sOPLS-AA density profiles strongly suggest that the polarization

effects (here estimated via the charge-scaling approach) contribute to the behavior observed in the interfacial tension ($\Delta\gamma < 0$). The different behavior for iodide salts is in good agreement with the expected behavior due to the well-known high polarizability of this anion.

**Table 2.** Summary of interfacial tension and interfacial tension differences ($\Delta\gamma = \gamma_{nHept/brine} - \gamma_{nHept/W}$; $\gamma_{nHept/W} = 52.401$ mN/m) for different aqueous phase compositions. The experimental data ($\Delta\gamma^{exp}$) is taken from Lima et al.[54]

| System | Force Field | $\gamma$ (mN/m) | $\Delta\gamma$ (mN/m) | $\Delta\gamma^{exp}$ (mN/m) |
|---|---|---|---|---|
| nHept/W | - | 52.401 | - | |
| nHept/NaCl | OPLS-AA | 54.079 | 1.678 | 1.5200 |
| | JC | 54.597 | 2.196 | |
| | sOPLS-AA | 53.2595 | 0.8585 | |
| nHept/NaI | OPLS-AA | 53.882 | 1.481 | -1.7620 |
| | JC | 54.518 | 2.117 | |
| | sOPLS-AA | 50.7135 | -1.6875 | |
| nHept/KCl | OPLS-AA | 54.023 | 1.622 | - |
| | JC | 54.246 | 1.845 | |
| | sOPLS-AA | 53.777 | 1.376 | |
| nHept/KI | OPLS-AA | 53.622 | 1.221 | -1.001 |
| | JC | 54.159 | 1.758 | |

| | | |
|---|---|---|
| sOPLS-AA | 50.629 | -1.772 |

Given the good qualitative performance in reproducing the experimental interfacial tension behavior, the remaining results and analyses are based on sOPLS-AA as the default force field (i.e., charge scaling of 0.85 applied to the ionic species).

*3.2 Interfacial properties of n-heptane/brine systems with surfactants*

*3.2.1 Structural properties*

Figure 2 shows the density profiles of the nHept/W system with 24 Span 80 and TED molecules at 298 K. As before, the simulations lead to smooth density profiles with well-characterized aqueous and oil bulk phases. As expected, water is not present in the n-heptane phase, and the surfactant molecules are mainly located at the n-heptane/water interface. Concerning the interfacial region, an abrupt transition around 4 to 6 nm is present, in which the surfactants are concentrated around 4.5 nm. A significant difference is observed when comparing the density distributions of Span 80 and TED, which can be attributed to the longer tail of Span 80. Also, the molecular structure of Span 80's tail slightly impacts the density profile of n-heptane molecules in the interfacial region, as observed when comparing Figures 2(a) and 2(b), and explicitly shown in Figure 2(c).

The structure of the surfactants in the nHept/W system can be further inspected by looking at the distributions of the surfactant heads and tails (Figure S4). In both systems, the surfactant heads are closer to the aqueous phase to maximize the water-surfactant interactions, while their tails are primarily located in the n-heptane-rich region of the interface. By comparing Figures 2 and S4, it is possible to explicitly notice that the broader distributions in Figure 2(a) are

mainly due to the surfactant tail distribution; it is worth mentioning that the more intense peak in the TED distribution is related to the higher molecular weight of the head as compared to Span 80.

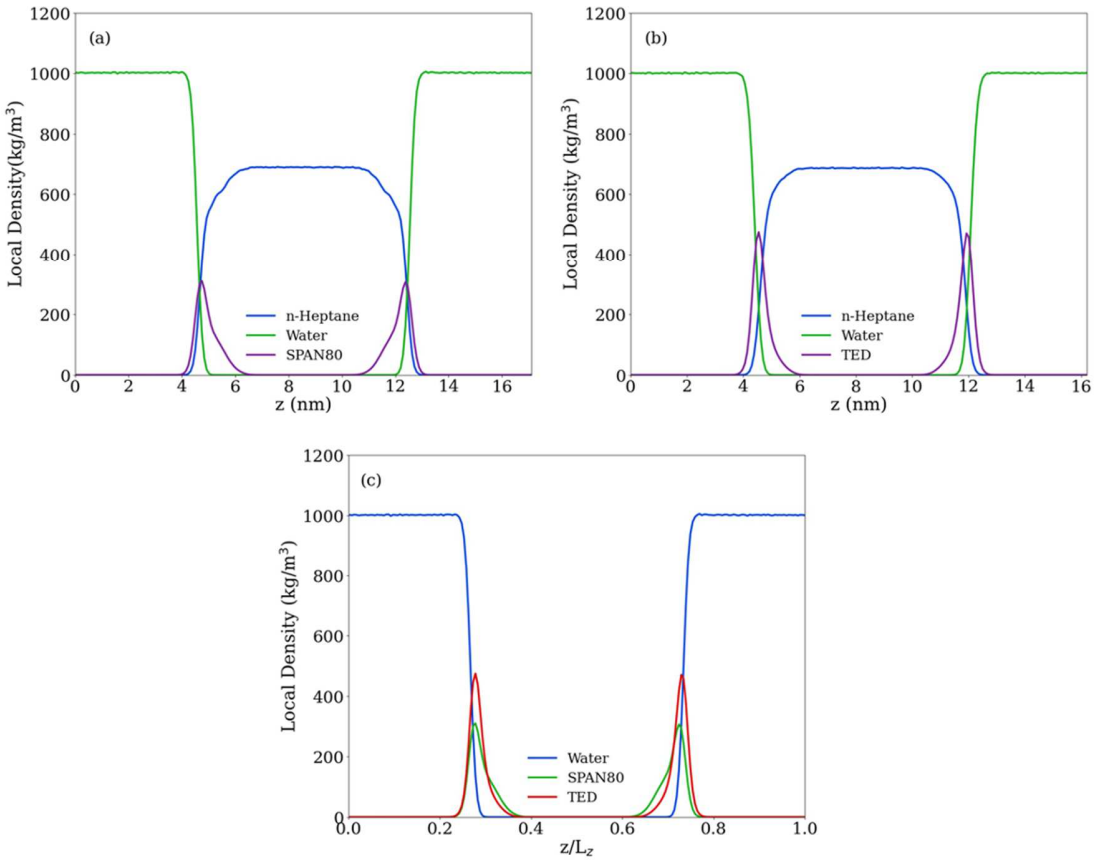


**Figure 2.** Density profiles of the nHept/W system with 24 molecules of: (a) Span 80 and (b) TED at 298 K. (c) Density Profiles of SPAN80 and TED are presented with the water profile for the nHept/W system as a function of $z/L_z$, in which $L_z$ is the z-dimension box length.

Figure 3 shows the influence of the brine phase composition on the interfacial behavior of the systems with 24 molecules of Span 80. Although it is possible to observe a slight difference

in the densities of the brine phase, the interfacial behavior is remarkably similar throughout the analyzed systems despite the different brine compositions. Namely, we find: (a) interfacial regions ranging from 4 nm to 6 nm; (b) no water solubility in the n-heptane phase and no n-heptane solubility in the aqueous phases; and (c) no surfactant solubilization is observed in either of the bulk phases. Very similar behavior is observed for TED, as shown in Figure S5, but with a slightly narrower interfacial region. Similar to the results presented for the surfactant-free interfacial systems, significant structuring of the ionic species near the interfacial regions are found for the nHept/NaI and nHept/KI systems.

The effect of increasing the number of Span 80 and TED on the interfacial structure is observed by comparing the density profiles with 24 surfactant molecules (Figures 2, 3, and S5) with those obtained for 48 surfactant molecules (Figures S6 and S7). In terms of the general solubility and ion structuring, a remarkable similarity is observed with the systems analyzed previously. Given the increased surfactant concentration, more pronounced peaks in the distributions of these compounds are shown in Figures S6 and S7. Also the previously observed effect introduced by the long tail of Span 80 becomes even more pronounced, while the increased surfactant concentration leads to a slightly smaller $I^-$ peak in the interfacial region.

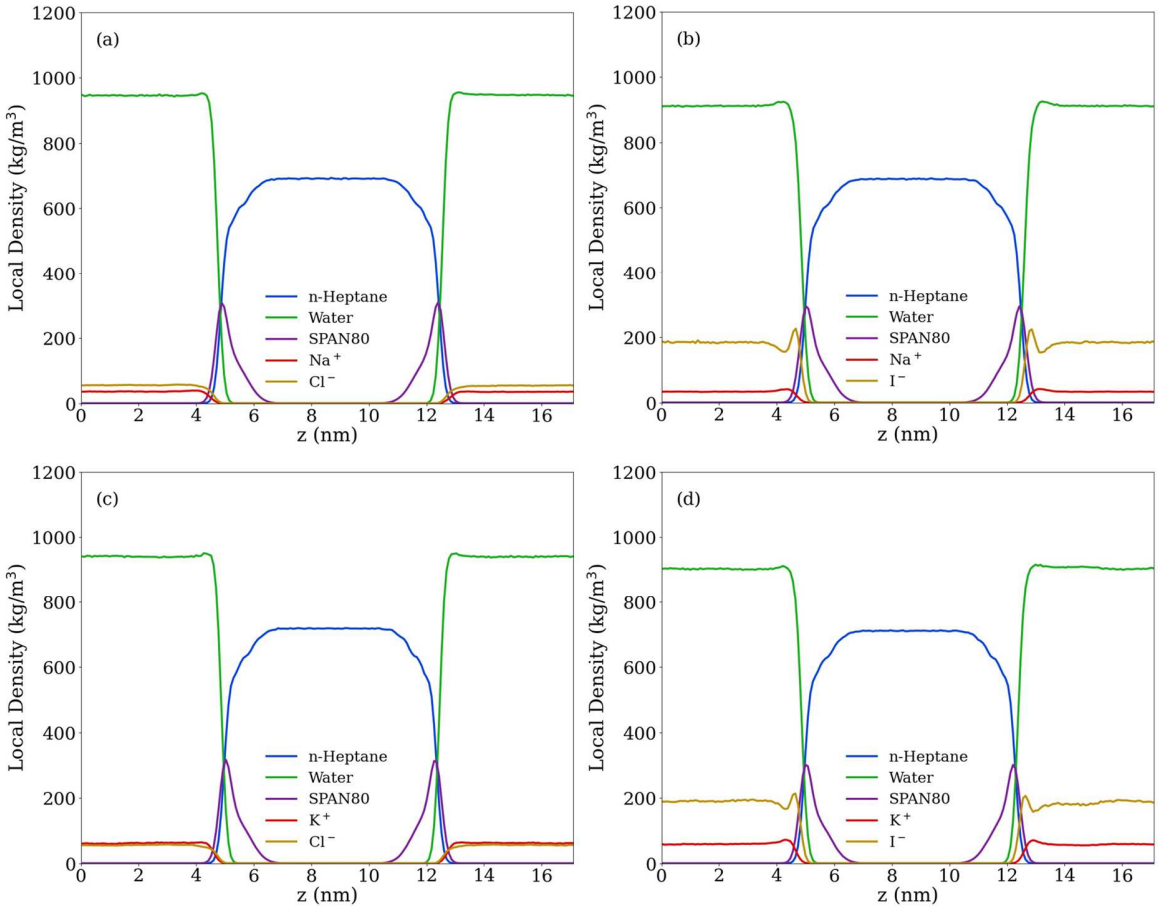


**Figure 3.** Density profiles of: (a) nHept/NaCl, (b) nHept/NaI, (c) nHept/KCl, and (d) nHept/KI with 24 molecules of Span 80 at 298 K.

As expected, the density profiles confirm that Span 80 and TED are preferentially located at the interface region. However, the local density distributions provide only partial information about the overall surfactant configurations at the interface. Figure 4 presents the results of the $S_z$ order parameter for the different interfacial systems with Span 80, in order to provide more structural details. For the nHept/W system with 24 surfactant molecules (Figure 4(a)), the surfactant tail ($\mathbf{v}_1$ and $\mathbf{v}_2$) shows a preferential parallel orientation, with an average angle of 95° between $\mathbf{v}_1$ and $\hat{\mathbf{e}}_\mathbf{z}$ and 125° between $\mathbf{v}_2$ and $\hat{\mathbf{e}}_\mathbf{z}$. The $\mathbf{v}_3$ vector, related to the polar portion of the

Span 80, also indicates an orientation parallel to the interface, with an angle between $\mathbf{v}_3$ and $\hat{\mathbf{e}}_z$ around 105°.

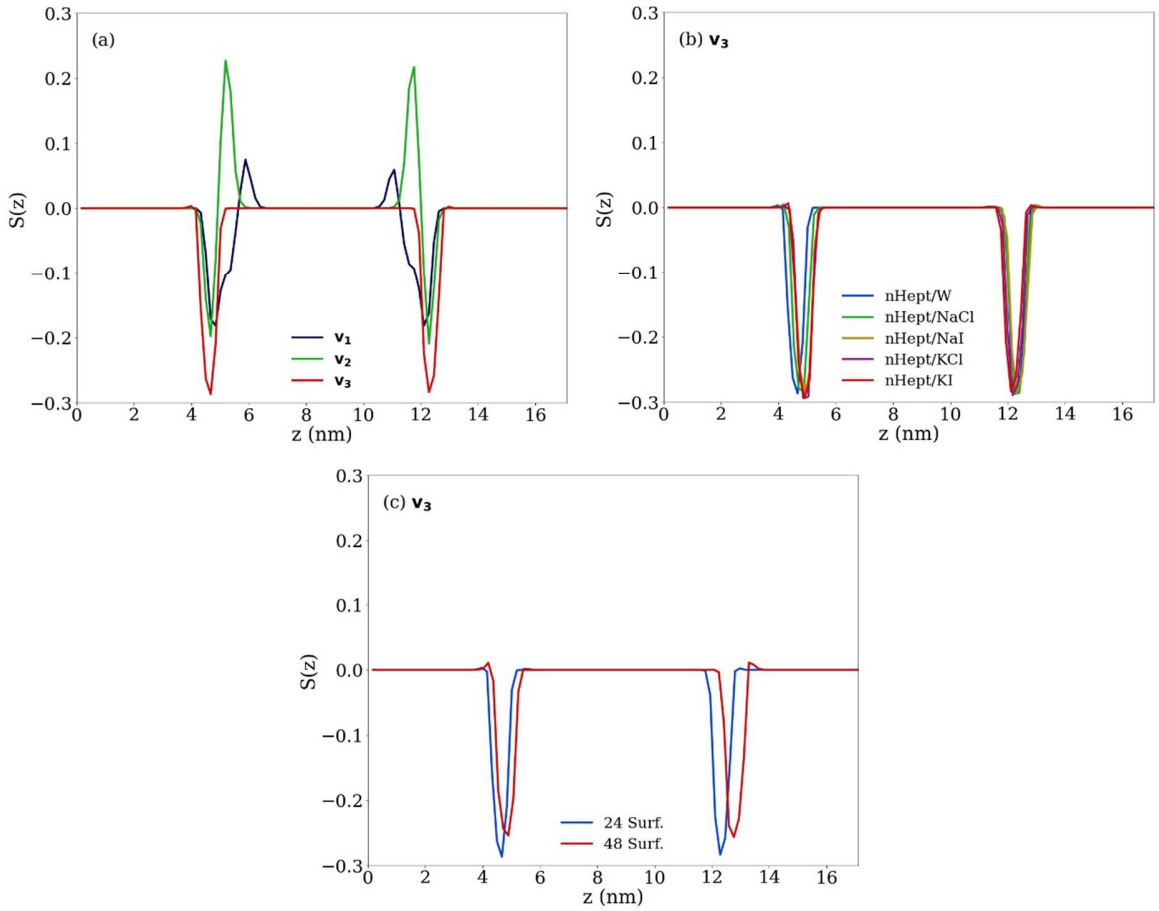


**Figure 4.** Order parameter along the z-axis for different interfacial systems with 24 ((a) and (b)) and 24/48 molecules (c) of Span 80. The predictions of (a) and (c) are made for the nHept/W system (no salts). The vector labels are consistent with Figure 1.

Interestingly, within the composition range evaluated here, the surfactant head orientation shows negligible sensitivity to the aqueous phase composition, as shown in Figure 4(b). The conformation of the tail and head of Span 80 parallel to the interface seems to suggest low interface saturation, leading to little penetration of the aqueous and oil phases. This is also

supported by looking at the S(z) profile presented in Figure 4(c); the tendency of the surfactant heads to orient parallel to the interface is slightly diminished by increasing the surfactant concentration.

Generally speaking, the S(z) profiles obtained for TED (Figure S7) are similar to those of Span 80. For instance, there is a pronounced parallel orientation of the TED tail and head portions, a low sensitivity to the aqueous phase composition, and a much more noticeable change when the surfactant concentration increases. Nonetheless, a slightly more parallel configuration to the interface is observed for TED, with angles of 115°, 95°, and 100° between $\mathbf{v}_1$ and $\hat{\mathbf{e}}_\mathbf{z}$, $\mathbf{v}_2$ and $\hat{\mathbf{e}}_\mathbf{z}$, and $\mathbf{v}_3$ and $\hat{\mathbf{e}}_\mathbf{z}$, respectively.

*3.2.2 Interfacial tension and interactions*

Table 3 shows the effect of the aqueous phase composition and surfactant concentration on the interfacial tension. In the nHept/W system, a significant reduction of $\gamma$ is observed by increasing the concentration of Span 80, as expected for amphiphilic compounds; similarly, by increasing the TED concentration, a decrease in interfacial tension of the nHept/W system is observed. TED leads to a more significant reduction in the interfacial tension, as expected, due to the smaller tail and the greater amount of hydrophilic groups in the TED head (versus Span 80). In the nHept/brine system, an increase in concentration of either surfactant decreases $\gamma$. However, for the systems containing NaCl and KCl, a slight increase occurs (i.e., $\Delta\gamma > 0$) as compared to the nHept/W system at the same surfactant concentrations. Interestingly, a cooperative effect is observed between the TED surfactants with NaI and KI. An analogous

result is obtained for the systems containing Span 80 and NaI; nonetheless, a negligible cooperation effect between Span 80 and KI is observed.

**Table 3.** Interfacial tension values as a function of the aqueous phase composition and surfactant concentration. $\Delta\gamma = \gamma_{N_{surf},nHept/brine} - \gamma_{ref}$, in which $\gamma_{ref} = \gamma_{N_{surf},nHept/W}$ for the nHept/brine systems and $\gamma_{ref} = \gamma_{,nHept/W}$ for nHept/W.

| System | Surf. | Span 80 | | TED | |
|---|---|---|---|---|---|
| | | $\gamma$ (mN/m) | $\Delta\gamma$ (mN/m) | $\gamma$ (mN/m) | $\Delta\gamma$ (mN/m) |
| nHept/W | 24 | 50.784 | -1.617 | 49.269 | -3.132 |
| | 48 | 48.091 | -4.310 | 43.159 | -9.241 |
| nHept/NaCl | 24 | 52.310 | 1.527 | 50.992 | 1.723 |
| | 48 | 49.180 | 1.089 | 44.622 | 1.462 |
| nHept/NaI | 24 | 49.330 | -1.454 | 49.059 | -0.210 |
| | 48 | 47.480 | -0.611 | 42.693 | -0.467 |
| nHep/KCl | 24 | 53.050 | 2.266 | 50.706 | 1.437 |
| | 48 | 49.580 | 1.489 | 44.287 | 1.128 |
| nHept/KI | 24 | 50.030 | -0.754 | 48.503 | -0.766 |
| | 48 | 48.210 | 0.119 | 43.137 | -0.022 |

Despite the cooperation between the surfactants and the iodide-based salts, as well as the accumulation of NaI and KI in the interfacial region, our results suggest negligible structural changes of the surfactants with respect to the different brine compositions. To further investigate the behavior, we analyzed the H-bonds between the surfactant and water molecules in the different interfacial systems. The results for the average H-bonds and H-bond lifetimes ($\tau_{HB}$) are presented in Table S1. As expected, the average number of H-bonds increases with the concentration of surfactants in all systems, but the correlation is not linear. This can be attributed to steric effects between the surfactant molecules, preventing the linear increase of associative interactions with additional water molecules. The average $\tau_{HB}$ shows only minor sensitivity to surfactant concentration. Interestingly, in all scenarios, both the number of H-bonds and $\tau_{HB}$ shows negligible sensitivity to the brine composition, suggesting that the ion structure at the interface does not influence the associative interactions between water and the surfactant molecules.

The individual contributions from the LJ and coulombic (Coul) interactions between Span 80 and water and Span 80 and n-heptane are presented in Table 4. As observed, the LJ contributions between Span 80 and n-heptane are significantly larger than those between Span 80 and water, but the LJ contributions between Span 80 and n-heptane do not change substantially with respect to the different aqueous phases. In contrast, the Coul interactions between Span 80

and water are much larger than the interactions between Span 80 and n-heptane. Moreover, the results in Table 4 suggest that electrostatic interactions primarily dominate Span 80-water interactions, which is expected due to the electronegative oxygen sites in the surfactant head. It is important to note that the Coul interactions between Span 80 and water are more sensitive to the aqueous phase composition than the LJ contributions. Similar behavior among the LJ and Coul contributions on the surfactant-water/n-heptane interactions is also present in the systems with TED (see Table S2). For instance, there is a more substantial LJ contribution for the interactions between TED and n-heptane, but there is a much more significant interaction for the TED-water Coul contribution, as well as greater sensitivity to the aqueous phase composition.

The behavior obtained for the interfacial tension due to different brine compositions can be further inspected by looking at the potential interactions presented in Tables 4 and S3. Interestingly, the systems in which there is a synergetic effect of the surfactants and ionic species (i.e., nHept/NaI and nHept/KI) present weaker potential energy interactions between water and surfactant molecules. The lower surfactant-water interactions in these systems suggests a more significant interaction between the surfactants and the ionic species, due to their accumulation in the interfacial region and their solvation by surfactant molecules. This observation is also corroborated by looking at Table S3, which shows more attractive interactions between the surfactant molecules and the cations and anions in the nHept/NaI and nHept/KI systems. This stronger interaction may contribute to the more pronounced concentration of surfactants in the interfacial region, which was also observed by Liu et al[65] when analyzing their experimental data on the synergetic surfactant/ion effects on the interfacial tension.

**Table 4.** LJ and Coul contributions and overall potential energies (U) between Span 80 and water, and Span 80 and n-heptane.

| System | Surf | LJ (kJ/mol) | | Coul (kJ/mol) | | U (kJ/mol) | |
|---|---|---|---|---|---|---|---|
| | | nHept | W | nHept | W | nHept | W |
| nHept/W | 24 | -3265.47 | -758.09 | -24.62 | -2736.07 | -3290.09 | -3494.16 |
| | 48 | -5465.62 | -1365.14 | -37.03 | -5128.27 | -5502.65 | -6493.41 |
| nHept/NaCl | 24 | -3285.87 | -731.91 | -24.50 | -2515.22 | -3310.37 | -3247.13 |
| | 48 | -5586.11 | -1314.78 | -38.24 | -4728.89 | -5624.35 | -6043.67 |
| nHept/NaI | 24 | -3265.10 | -670.08 | -22.08 | -2327.19 | -3287.18 | -2997.27 |
| | 48 | -5601.46 | -1223.51 | -35.46 | -4410.52 | -5636.92 | -5634.03 |
| nHept/KCl | 24 | -3452.01 | -741.08 | -26.98 | -2541.72 | -3478.99 | -3282.80 |
| | 48 | -5614.71 | -1290.46 | -37.91 | -4679.72 | -5652.62 | -5970.18 |
| nHept/KI | 24 | -3434.04 | -684.34 | -24.75 | -2397.92 | -3458.79 | -3082.26 |
| | 48 | -5622.81 | -1227.90 | -35.95 | -4524.27 | -5658.76 | -5752.17 |

*3.3.3 Potential of mean force*

Finally, we analyzed the interfacial behavior of Span 80 and TED surfactants in different interfacial systems by examining the PMFs as a function of the z-component of the center-of-mass distance between a single surfactant molecule and the n-heptane rich phase (Figure 5).

Based on these PMFs, the transfer free energy of the surfactant molecules throughout the different phases, including the interfacial region, is directly obtained (Table 5).

The approach used here produces smooth PMFs, with narrow statistical confidence regions and well-characterized n-heptane and aqueous phases. The non-ionic surfactants show more favorable solubility in the n-heptane phase than in the different brine phases. Smaller $\Delta G^{nHept/A}$ for TED indicates that TED is slightly more hydrophilic than Span 80. When transferring TED or Span 80 from the n-heptane phase to the interface ($\Delta G^{nHept/I}$), there is some minor sensitivity to the different compositions of the aqueous phase. $\Delta G^{nHept/I}$ for TED is significantly smaller than that obtained for Span 80, which is consistent with TED's higher hydrophilicity. Conversely, a pronounced salting-out effect is observed when comparing $\Delta G^{nHept/A}$ for the nHept/W systems with the nHept/brine systems. For TED transfer, the value of $\Delta G^{nHept/A}$ is relatively unaffected by the presence of NaI and KI, due to the statistically negligible difference between these systems and nHept/W, as can be seen in Figure 5(b).

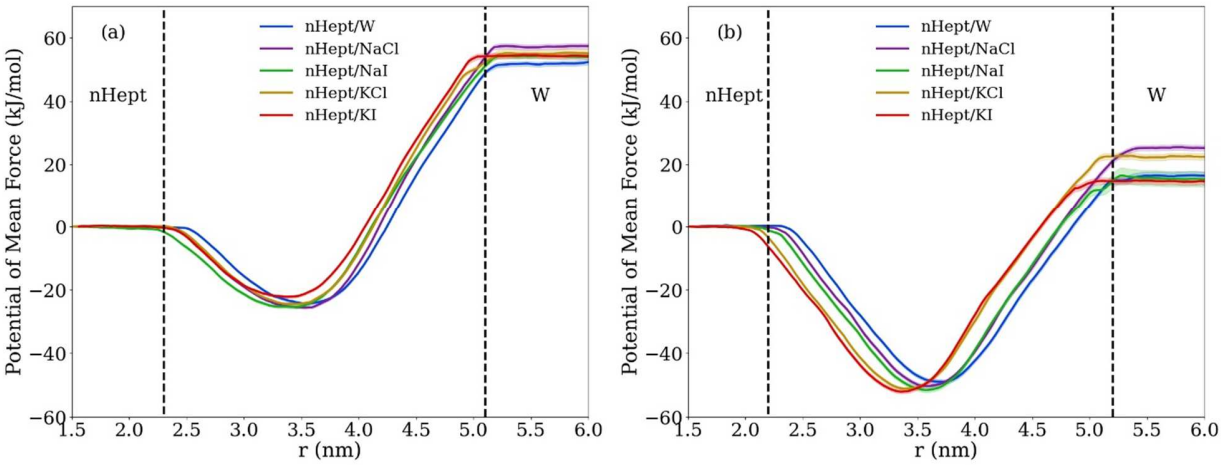


**Figure 5.** PMFs of: (a) Span 80 and (b) TED as a function of the center-of-mass distance between a single surfactant molecule and the n-heptane phase along the z-dimension of the simulation box at 298 K and 1 bar. The shaded areas represents the statistical confidence, predicted using bootstrap analysis, and the dashed vertical lines indicate approximate phase boundaries.

An analysis of the surfactant transfer free energy from the aqueous phase to the interfacial region ($\Delta G^{W/I}$) can also be correlated to the synergetic behavior of the interfacial tension identified earlier (Table 3). With respect to the current surfactants, composition range, and thermodynamic conditions, we obtain slightly lower values of $\Delta G^{W/I}$ for the nHept/NaCl and nHept/KCl systems, as compared to other brines. This suggests a more favorable surfactant transfer to the interfacial region when compared to the other evaluated systems. Conversely, in the systems exhibiting synergetic behavior (NaI and KI), a slightly larger $\Delta G^{W/I}$ is obtained. These results may seem counterintuitive when compared with the LJ and Coul contributions (Table 4 and S3). However, the PMFs were calculated in systems with a single surfactant molecule. Thus, these results suggest that beyond the surfactant-ion interaction, the interaction between surfactant molecules also plays an important role in the surfactant adsorption and

interfacial tension behavior. The PMF results suggest that NaI and KI not only interact with the surfactant molecules but also contribute to the surfactant-surfactant interaction. This hypothesis is also corroborated by looking at the average surfactant-surfactant potential energy in the interfacial systems, as shown in Table S4.

**Table 5.** Transfer free energy (kJ/mol) of a single surfactant molecule in the interfacial systems at 298 K and 1 bar. The first superscript indicates the initial phase location, and the second superscript indicates the final phase location ($\Delta G^{P1/P2} = G^{P2} - G^{P1}$).

| System | Span 80 | | | TED | | |
|---|---|---|---|---|---|---|
| | $\Delta G^{nHept/A}$ | $\Delta G^{A/I}$ | $\Delta G^{nHept/I}$ | $\Delta G^{nHept/A}$ | $\Delta G^{A/I}$ | $\Delta G^{nHept/I}$ |
| nHept/W | 52.581 | -76.912 | -24.332 | 16.507 | -65.502 | -48.994 |
| nHept/NaCl | 58.029 | -83.590 | -25.561 | 25.817 | -76.141 | -50.324 |
| nHept/NaI | 54.366 | -79.753 | -25.387 | 16.415 | -67.981 | -51.566 |
| nHept/KCl | 55.975 | -80.405 | -24.430 | 22.701 | -73.858 | -51.156 |
| nHept/KI | 55.483 | -77.627 | -22.145 | 15.208 | -67.290 | -52.081 |

## 4. Final Remarks

In this work, MD simulations are used to investigate the synergistic effects on the interfacial properties between nonionic surfactants and ionic species. When initially analyzing the interfacial n-heptane/brine systems without surfactants, we obtained excellent qualitative and quantitative agreement with experimental interfacial tension data. However, this required applying a charge scaling factor of 0.85 to the ionic species, suggesting that it is important to account for polarizability effects of ionic species when predicting interfacial properties of similar systems.

Tensoactive behavior is observed for the NaI and KI systems, and these systems are also found to exhibit noticeable layering of the iodide species near the interface. When comparing the two different surfactants (Span 80 versus TED), the Span 80 surfactant protrudes much more noticeably into the n-heptane phase, primarily due to its longer alkane tail. There are significant interaction differences (average potential energy) between the surfactants and the different ionic species. However, the structure of the surfactants (orientation distributions; density profiles) and thermodynamic behavior (transfer free energies) remain robust and are relatively unaffected by the specific salt species present. Furthermore, the H-bonding characteristics between the surfactants and water are very stable, despite the presence of the different salts.

An analysis of the LJ and Coul contributions, as well as the PMFs, suggest that the surfactant-surfactant interactions play a critical role in maintaining stability within the interfacial structure, with a much smaller impact associated with the composition of the different brine solutions.

**Acknowledgements**

This work is partially supported by the Alabama Advanced Solvent Cluster (AASC), funded by the U.S. Department of Energy Established Program to Stimulate Competitive Research (DOE-EPSCoR) (DE-SC0020282).

**References**


(1) Massarweh, O.; Abushaikha, A. S. The Use of Surfactants in Enhanced Oil Recovery: A Review of Recent Advances. *Energy Rep.* **2020**, *6*, 3150–3178. https://doi.org/10.1016/j.egyr.2020.11.009.

(2) Belhaj, A. F.; Elraies, K. A.; Mahmood, S. M.; Zulkifli, N. N.; Akbari, S.; Hussien, O. S. The Effect of Surfactant Concentration, Salinity, Temperature, and PH on Surfactant Adsorption for Chemical Enhanced Oil Recovery: A Review. *J. Pet. Explor. Prod. Technol.* **2020**, *10* (1), 125–137. https://doi.org/10.1007/s13202-019-0685-y.

(3) Isaac, O. T.; Pu, H.; Oni, B. A.; Samson, F. A. Surfactants Employed in Conventional and Unconventional Reservoirs for Enhanced Oil Recovery—A Review. *Energy Rep.* **2022**, *8*, 2806–2830. https://doi.org/10.1016/j.egyr.2022.01.187.

(4) Bonto, M.; Eftekhari, A. A.; Nick, H. M. An Overview of the Oil-Brine Interfacial Behavior and a New Surface Complexation Model. *Sci. Rep.* **2019**, *9* (1), 6072. https://doi.org/10.1038/s41598-019-42505-2.

(5) Rostami, P.; Mehraban, M. F.; Sharifi, M.; Dejam, M.; Ayatollahi, S. Effect of Water Salinity on Oil/Brine Interfacial Behaviour during Low Salinity Waterflooding: A Mechanistic Study. *Petroleum* **2019**, *5* (4), 367–374. https://doi.org/10.1016/j.petlm.2019.03.005.

(6) Zolfaghari, R.; Fakhru'l-Razi, A.; Abdullah, L. C.; Elnashaie, S. S. E. H.; Pendashteh, A. Demulsification Techniques of Water-in-Oil and Oil-in-Water Emulsions in Petroleum Industry. *Sep. Purif. Technol.* **2016**, *170*, 377–407. https://doi.org/10.1016/j.seppur.2016.06.026.

(7) Rahate, A. R.; Nagarkar, J. M. Emulsification of Vegetable Oils Using a Blend of Nonionic Surfactants for Cosmetic Applications. *J. Dispers. Sci. Technol.* **2007**, *28* (7), 1077–1080. https://doi.org/10.1080/01932690701524802.

(8) Yan, D.; Meng, L.; Li, H.; Song, T.; Sun, P.; Bao, M.; Li, X. Petroleum Hydrocarbon Release Behavior Study in Oil-Sediment Aggregates: Turbulence Intensity and Chemical Dispersion Effect. *RSC Adv.* **2019**, *9* (14), 7922–7931. https://doi.org/10.1039/C8RA08871C.

(9) Ash, D.; Majee, S. B.; Biswas, G. R. SPAN 40/TWEEN 80-BASED SOYBEAN OLEOGELS: MODELING OF GELATION KINETICS AND DRUG RELEASE. *Int. J. Pharm. Sci. Res.* **2019** *10* (10) 1000-09.

(10) Chen, S.; Hanning, S.; Falconer, J.; Locke, M.; Wen, J. Recent Advances in Non-Ionic Surfactant Vesicles (Niosomes): Fabrication, Characterization, Pharmaceutical and Cosmetic Applications. *Eur. J. Pharm. Biopharm.* **2019**, *144*, 18–39. https://doi.org/10.1016/j.ejpb.2019.08.015.

(11) Benmekhbi, M.; Simon, S.; Sjöblom, J. Dynamic and Rheological Properties of Span 80 at Liquid–Liquid Interfaces. *J. Dispers. Sci. Technol.* **2014**, *35* (6), 765–776. https://doi.org/10.1080/01932691.2013.811573.

(12) Pandolfini, P.; Loglio, G.; Ravera, F.; Liggieri, L.; Kovalchuk, V. I.; Javadi, A.; Karbaschi, M.; Krägel, J.; Miller, R.; Noskov, B. A.; Bykov, A. G. Dynamic Properties of Span-80 Adsorbed Layers at Paraffin-Oil/Water Interface: Capillary Pressure Experiments under Low Gravity Conditions. *Colloids Surf. Physicochem. Eng. Asp.* **2017**, *532*, 228–243. https://doi.org/10.1016/j.colsurfa.2017.05.012.

(13) Owusu Apenten, R. K.; Zhu, Q.-H. Interfacial Parameters for Selected Spans and Tweens at the Hydrocarbon—Water Interface. *Food Hydrocoll.* **1996**, *10* (1), 27–30. https://doi.org/10.1016/S0268-005X(96)80050-6.

(14) Santini, E.; Liggieri, L.; Sacca, L.; Clausse, D.; Ravera, F. Interfacial Rheology of Span 80 Adsorbed Layers at Paraffin Oil–Water Interface and Correlation with the Corresponding Emulsion Properties. *Colloids Surf. Physicochem. Eng. Asp.* **2007**, *309* (1–3), 270–279. https://doi.org/10.1016/j.colsurfa.2006.11.041.

(15) Capdevila, M.; Maestro, A.; Porras, M.; Gutiérrez, J. M. Preparation of Span 80/Oil/Water Highly Concentrated Emulsions: Influence of Composition and Formation Variables and Scale-Up. *J. Colloid Interface Sci.* **2010**, *345* (1), 27–33. https://doi.org/10.1016/j.jcis.2010.01.045.

(16) Bąk, A.; Podgórska, W. Interfacial and Surface Tensions of Toluene/Water and Air/Water Systems with Nonionic Surfactants Tween 20 and Tween 80. *Colloids Surf. Physicochem. Eng. Asp.* **2016**, *504*, 414–425. https://doi.org/10.1016/j.colsurfa.2016.05.091.

(17) Cao, G.; Du, T.; Bai, Y.; Yang, T.; Zuo, J. Effects of Surfactant Molecular Structure on the Stability of Water in Oil Emulsion. *J. Pet. Sci. Eng.* **2021**, *196*, 107695. https://doi.org/10.1016/j.petrol.2020.107695.

(18) Lv, G.; Wang, F.; Cai, W.; Zhang, X. Characterization of the Addition of Lipophilic Span 80 to the Hydrophilic Tween 80-Stabilized Emulsions. *Colloids Surf. Physicochem. Eng. Asp.* **2014**, *447*, 8–13. https://doi.org/10.1016/j.colsurfa.2014.01.066.

(19) Koroleva, S. V.; Korchak, P.; Victorov, A. I. Molecular Thermodynamic Modeling of the Specific Effect of Salt on the Aggregation of Nonionic Surfactants. *J. Chem. Eng. Data* **2020**, *65* (3), 987–992. https://doi.org/10.1021/acs.jced.9b00303.

(20) Carale, T. R.; Pham, Q. T.; Blankschtein, D. Salt Effects on Intramicellar Interactions and Micellization of Nonionic Surfactants in Aqueous Solutions. *Langmuir* **1994**, *10* (1), 109–121. https://doi.org/10.1021/la00013a016.

(21) Al-Sabagh, A. M.; Nasser, N. M.; Migahed, M. A.; Kandil, N. G. Effect of Chemical

Structure on the Cloud Point of Some New Non-Ionic Surfactants Based on Bisphenol in Relation to Their Surface Active Properties. *Egypt. J. Pet.* **2011**, *20* (2), 59–66. https://doi.org/10.1016/j.ejpe.2011.06.006.

(22) Hadji, M.; Aoudia, M.; Al-Rubkhi, A.; Al-Maamari, R. S.; Hadj-Ziane-Zafour, A. Effect of Sodium Carbonate on the Cloud Point in Alkyl Ether/Brine Systems: Apparent Relation with Dynamic Interfacial Tension Minimum. *J. Surfactants Deterg.* **2016**, *19* (6), 1223–1229. https://doi.org/10.1007/s11743-016-1870-3.

(23) Imperatore, R.; Vitiello, G.; Ciccarelli, D.; D'Errico, G. Effects of Salts on the Micellization of a Short-Tailed Nonionic Ethoxylated Surfactant: An Intradiffusion Study. *J. Solut. Chem.* **2014**, *43* (1), 227–239. https://doi.org/10.1007/s10953-014-0133-z.

(24) Alotaibi, M. B.; Cha, D.; Chand, K.; Yousef, A. A. Effects of Ions on the Characteristics of Monolayer at Brine/Oil Interfaces. *E3S Web Conf.* **2019**, *89*, 04003. https://doi.org/10.1051/e3sconf/20198904003.

(25) Katiyar, P.; Singh, J. K. A Coarse-Grain Molecular Dynamics Study of Oil–Water Interfaces in the Presence of Silica Nanoparticles and Nonionic Surfactants. *J. Chem. Phys.* **2017**, *146* (20), 204702. https://doi.org/10.1063/1.4984073.

(26) Jiang, X.; Liu, M.; Li, X.; Wang, L.; Liang, S.; Guo, X. Effects of Surfactant and Hydrophobic Nanoparticles on the Crude Oil-Water Interfacial Tension. *Energies* **2021**, *14* (19), 6234. https://doi.org/10.3390/en14196234.

(27) Li, N.; Sun, Z.; Pang, Y.; Qi, Z.; Liu, W.; Li, W.; Sun, M.; Li, B.; Wang, Z. Microscopic Mechanism for Electrocoalescence of Water Droplets in Water-in-Oil Emulsions Containing Surfactant: A Molecular Dynamics Study. *Sep. Purif. Technol.* **2022**, *289*, 120756. https://doi.org/10.1016/j.seppur.2022.120756.

(28) Kang, B.; Tang, H.; Zhao, Z.; Song, S. Hofmeister Series: Insights of Ion Specificity from Amphiphilic Assembly and Interface Property. *ACS Omega* **2020**, *5* (12), 6229–6239. https://doi.org/10.1021/acsomega.0c00237.

(29) Moghaddam, S. Z.; Thormann, E. The Hofmeister Series: Specific Ion Effects in Aqueous Polymer Solutions. *J. Colloid Interface Sci.* **2019**, *555*, 615–635. https://doi.org/10.1016/j.jcis.2019.07.067.

(30) Kikkawa, N.; Wang, L.; Morita, A. Computational Study of Effect of Water Finger on Ion Transport through Water-Oil Interface. *J. Chem. Phys.* **2016**, *145* (1), 014702. https://doi.org/10.1063/1.4954774.

(31) Underwood, T. R.; Greenwell, H. C. The Water-Alkane Interface at Various NaCl Salt Concentrations: A Molecular Dynamics Study of the Readily Available Force Fields. *Sci. Rep.* **2018**, *8* (1), 352. https://doi.org/10.1038/s41598-017-18633-y.

(32) Abdel-Azeim, S.; Sakthivel, S.; Kandiel, T. A.; Kanj, M. Y. Specificity and Synergy at the Oil–Brine Interface: New Insights from Experiments and Molecular Dynamics Simulations. *Energy Fuels* **2021**, *35* (18), 14647–14657. https://doi.org/10.1021/acs.energyfuels.1c02133.

(33) Nan, Y.; Li, W.; Jin, Z. Ion Valency and Concentration Effect on the Structural and Thermodynamic Properties of Brine–Decane Interfaces with Anionic Surfactant (SDS). *J. Phys. Chem. B* **2021**, *125* (33), 9610–9620. https://doi.org/10.1021/acs.jpcb.1c04187.

(34) Riccardi, E.; Tichelkamp, T. Calcium Ion Effects on the Water/Oil Interface in the Presence of Anionic Surfactants. *Colloids Surf. Physicochem. Eng. Asp.* **2019**, *573*, 246–254. https://doi.org/10.1016/j.colsurfa.2019.04.001.

(35) Alonso, G.; Gamallo, P.; Mejía, A.; Sayós, R. Assessing Salt-Surfactant Synergistic Effects on Interfacial Tension from Molecular Dynamics Simulations. *J. Mol. Liq.* **2020**, *299*, 112223. https://doi.org/10.1016/j.molliq.2019.112223.

(36) Lindahl; Abraham; Hess; Spoel, van der. GROMACS 2021.1 Manual. **2021**. https://doi.org/10.5281/ZENODO.4561625.

(37) Lindahl; Abraham; Hess; Spoel, van der. GROMACS 2021.1 Source Code. **2021**. https://doi.org/10.5281/ZENODO.4561626.

(38) Dodda, L. S.; de Vaca, I.; Tirado-Rives, J.; Jorgensen, W. L. LigParGen Web Server: An Automatic OPLS-AA Parameter Generator for Organic Ligands. *Nucleic Acids Res.* **2017**, *45* (W1), W331-W336.

(39) Jorgensen, W. L.; Maxwell, D. S.; Tirado-Rives, J. Development and Testing of the OPLS All-Atom Force Field on Conformational Energetics and Properties of Organic Liquids. *J. Am. Chem. Soc.* **1996**, *118* (45), 11225–11236.

(40) Jorgensen, W. L.; Tirado-Rives, J. The OPLS Force Field for Proteins. Energy Minimizations for Crystals of Cyclic Peptides and Crambin. *J. Am. Chem. Soc.* **1988**, *110* (6), 1657–1666.

(41) Berendsen, H. J. C.; Grigera, J. R.; Straatsma, T. P. The Missing Term in Effective Pair Potentials. *J. Phys. Chem.* **1987**, *91* (24), 6269–6271. https://doi.org/10.1021/j100308a038.

(42) Frisch, M. J.; Trucks, G. W.; Schlegel, H. B.; Scuseria, G. E.; Cheeseman, J. R.; Scalmani, G.; Barone, V.; Mennucci, B.; Petersson, G. A. Gaussian 09, revision D.01.

(43) Dodda, L. S.; Vilseck, J. Z.; Cutrona, K. J.; Jorgensen, W. L. Evaluation of CM5 Charges for Nonaqueous Condensed-Phase Modeling. *J. Chem. Theory Comput.* **2015**, *11* (9), 4273–4282. https://doi.org/10.1021/acs.jctc.5b00414.

(44) Marenich, A. V.; Jerome, S. V.; Cramer, C. J.; Truhlar, D. G. Charge Model 5: An Extension of Hirshfeld Population Analysis for the Accurate Description of Molecular Interactions in Gaseous and Condensed Phases. *J. Chem. Theory Comput.* **2012**, *8* (2), 527–541. https://doi.org/10.1021/ct200866d.

(45) Darden, T.; York, D.; Pedersen, L. Particle Mesh Ewald: An Nlog (N) Method for Ewald Sums in Large Systems. *J. Chem. Phys.* **1993**, *98* (12), 10089–10092.

(46) Åqvist, J. Ion-Water Interaction Potentials Derived from Free Energy Perturbation Simulations. *J. Phys. Chem.* **1990**, *94* (21), 8021–8024. https://doi.org/10.1021/j100384a009.

(47) Lybrand, T. P.; Ghosh, I.; McCammon, J. A. Hydration of Chloride and Bromide Anions: Determination of Relative Free Energy by Computer Simulation. *J. Am. Chem. Soc.* **1985**, *107* (25), 7793–7794. https://doi.org/10.1021/ja00311a112.

(48) Chandrasekhar, J.; Spellmeyer, D. C.; Jorgensen, W. L. Energy Component Analysis for Dilute Aqueous Solutions of $Li^+$, $Na^+$, $F^-$, and $Cl^-$ Ions. *J. Am. Chem. Soc.* **1984**, *106* (4), 903–910. https://doi.org/10.1021/ja00316a012.

(49) Joung, I. S.; Cheatham, T. E. Determination of Alkali and Halide Monovalent Ion Parameters for Use in Explicitly Solvated Biomolecular Simulations. *J. Phys. Chem. B* **2008**, *112* (30), 9020–9041. https://doi.org/10.1021/jp8001614.

(50) Zeron, I. M.; Abascal, J. L. F.; Vega, C. A Force Field of $Li^+$, $Na^+$, $K^+$, $Mg^{2+}$, $Ca^{2+}$, $Cl^-$, and $SO_4^{2-}$ in Aqueous Solution Based on the TIP4P/2005 Water Model and Scaled Charges for the Ions. *J. Chem. Phys.* **2019**, *151* (13), 134504. https://doi.org/10.1063/1.5121392.

(51) Leontyev, I. V.; Stuchebrukhov, A. A. Electronic Continuum Model for Molecular Dynamics Simulations of Biological Molecules. *J. Chem. Theory Comput.* **2010**, *6* (5), 1498–1508. https://doi.org/10.1021/ct9005807.

(52) Barbosa, G. D.; Liu, X.; O'Harra, K. E.; Bara, J. E.; Turner, C. H. Charge Scaling Parameter Evaluation for Multivalent Ionic Liquids with Fixed Point Charge Force Fields. *J. Ion. Liq.* **2022**, *2* (1), 100020. https://doi.org/10.1016/j.jil.2022.100020.

(53) Martinez, L.; Andrade, R.; Birgin, E. G.; Martinez, J. M. PACKMOL: A Package for Building Initial Configurations for Molecular Dynamics Simulations. *J. Comput. Chem.* **2009**, *30* (13), 2157–2164.

(54) Lima, E. R. A.; Melo, B. M. de; Baptista, L. T.; Paredes, M. L. L. Specific Ion Effects on the Interfacial Tension of Water/Hydrocarbon Systems. *Braz. J. Chem. Eng.* **2013**, *30* (1), 55–62. https://doi.org/10.1590/S0104-66322013000100007.

(55) Nosé, S.; Klein, M. L. Constant Pressure Molecular Dynamics for Molecular Systems. *Mol.*

*Phys.* **1983**, *50* (5), 1055–1076.

(56) Parrinello, M.; Rahman, A. Polymorphic Transitions in Single Crystals: A New Molecular Dynamics Method. *J. Appl. Phys.* **1981**, *52* (12), 7182–7190.

(57) Bussi, G.; Donadio, D.; Parrinello, M. Canonical Sampling through Velocity Rescaling. *J. Chem. Phys.* **2007**, *126* (1), 14101.

(58) de Lara, L. S.; Michelon, M. F.; Miranda, C. R. Molecular Dynamics Studies of Fluid/Oil Interfaces for Improved Oil Recovery Processes. *J. Phys. Chem. B* **2012**, *116* (50), 14667–14676. https://doi.org/10.1021/jp310172j.

(59) Torrie, G. M.; Valleau, J. P. Nonphysical Sampling Distributions in Monte Carlo Free-Energy Estimation: Umbrella Sampling. *J. Comput. Phys.* **1977**, *23* (2), 187–199. https://doi.org/10.1016/0021-9991(77)90121-8.

(60) Kumar, S.; Rosenberg, J. M.; Bouzida, D.; Swendsen, R. H.; Kollman, P. A. THE Weighted Histogram Analysis Method for Free-Energy Calculations on Biomolecules. I. The Method. *J. Comput. Chem.* **1992**, *13* (8), 1011–1021. https://doi.org/10.1002/jcc.540130812.

(61) Engin, O.; Villa, A.; Sayar, M.; Hess, B. Driving Forces for Adsorption of Amphiphilic Peptides to the Air−Water Interface. *J. Phys. Chem. B* **2010**, *114* (34), 11093–11101. https://doi.org/10.1021/jp1024922.

(62) Hub, J. S.; de Groot, B. L.; van der Spoel, D. g_wham—A Free Weighted Histogram Analysis Implementation Including Robust Error and Autocorrelation Estimates. *J. Chem. Theory Comput.* **2010**, *6* (12), 3713–3720. https://doi.org/10.1021/ct100494z.

(63) Yarranton, H. W.; Alboudwarej, H.; Jakher, R. Investigation of Asphaltene Association with Vapor Pressure Osmometry and Interfacial Tension Measurements. *Ind. Eng. Chem. Res.* **2000**, *39* (8), 2916–2924. https://doi.org/10.1021/ie000073r.

(64) Li, B.; Fu, J. Interfacial Tensions of Two-Liquid-Phase Ternary Systems. *J. Chem. Eng. Data* **1992**, *37* (2), 172–174. https://doi.org/10.1021/je00006a009.

(65) Liu, Z.-Y.; Li, Z.-Q.; Song, X.-W.; Zhang, J.-C.; Zhang, L.; Zhang, L.; Zhao, S. Dynamic Interfacial Tensions of Binary Nonionic–Anionic and Nonionic Surfactant Mixtures at Water–Alkane Interfaces. *Fuel* **2014**, *135*, 91–98. https://doi.org/10.1016/j.fuel.2014.06.031.

## Graphical Abstract